Automated mitotic spindle tracking suggests a link between spindle dynamics, spindle orientation, and anaphase onset in epithelial cells

Matthew E. Larson[a,b,c,*] and William M. Bement[a,b,c,d,*]
[a]Medical Scientist Training Program, [b]Cellular and Molecular Biology Graduate Program, [c]Laboratory of Cell and Molecular Biology, and [d]Department of Zoology, University of Wisconsin–Madison, Madison, WI 53706

ABSTRACT **Proper spindle positioning at anaphase onset is essential for normal tissue organization and function. Here we develop automated spindle-tracking software and apply it to characterize mitotic spindle dynamics in the *Xenopus laevis* embryonic epithelium. We find that metaphase spindles first undergo a sustained rotation that brings them on-axis with their final orientation. This sustained rotation is followed by a set of striking stereotyped rotational oscillations that bring the spindle into near contact with the cortex and then move it rapidly away from the cortex. These oscillations begin to subside soon before anaphase onset. Metrics extracted from the automatically tracked spindles indicate that final spindle position is determined largely by cell morphology and that spindles consistently center themselves in the *XY*-plane before anaphase onset. Finally, analysis of the relationship between spindle oscillations and spindle position relative to the cortex reveals an association between cortical contact and anaphase onset. We conclude that metaphase spindles in epithelia engage in a stereotyped "dance," that this dance culminates in proper spindle positioning and orientation, and that completion of the dance is linked to anaphase onset.**

Monitoring Editor
Stephen Doxsey
University of Massachusetts

Received: Jun 3, 2016
Revised: Nov 28, 2016
Accepted: Jan 11, 2017

INTRODUCTION

Spindle positioning is one of the most consequential events in the cell division cycle: the position of the spindle determines whether the division is symmetric or asymmetric, whether localized developmental information is equally or unequally distributed to the daughter cells, and whether the daughter cells are positioned within or outside of the tissue of their origin. All of these outcomes follow from spindle positioning via a deceptively simple rule—the midplane of the anaphase spindle defines the cleavage plane. Thus understanding the dynamic processes that lead to anaphase spindle positioning is a major goal of both cell and developmental biology (Morin and Bellaïche, 2011; Nestor-Bergmann *et al.*, 2014).

Much of our information concerning spindle positioning derives from studies of asymmetric cell division in epithelia, the most common tissue type (reviewed in Knoblich, 2001, 2008; Morin and Bellaïche, 2011). Asymmetric cell division in epithelia is commonly used to unequally partition developmental information and thereby direct specification of a nonepithelial fate for one of the two daughter cells (Betschinger and Knoblich, 2004). However, symmetric cell division is arguably just as important, particularly in epithelia, where it is the primary mode of division and in which spindle position deficits are associated with diseases. For example, analysis of fixed epithelial cells from mouse intestine (Fleming *et al.*, 2007) or developing kidney (Fischer *et al.*, 2006) showed that >95% of spindles normally assume an orientation parallel to the plane of the epithelium (i.e., a "planar" orientation) before division. Strikingly, this planar spindle orientation is significantly reduced in the same cell types in corresponding pathologies—intestinal tumors (Fleming *et al.*, 2009) and polycystic kidney disease (Fischer *et al.*, 2006), respectively.

In some circumstances, the orientation of the spindle during symmetric division is directed as part of an ongoing developmental process (Baena-López *et al.*, 2005; da Silva and Vincent, 2007; Castanon *et al.*, 2013). In other systems, no direct regulation of orientation has been established. However, it has long been observed that spindles have a tendency to orient along the long axis of the cell

This article was published online ahead of print in MBoC in Press (http://www.molbiolcell.org/cgi/doi/10.1091/mbc.E16-06-0355) on January 18, 2017.
*Address correspondence to: Matt Larson (melarson3@wisc.edu), Bill Bement (wmbement@wisc.edu).
Abbreviations used: GUI, graphical user interface; RMS, root mean square error.

(Hertwig, 1884; O'Connell and Wang, 2000; Strauss *et al.*, 2006). Further, spindles in cultured cells plated on patterned substrates orient along the force axis of the cell (Théry *et al.*, 2005, 2007), suggesting that mitotic spindles may also orient along force gradients in intact tissues (Nestor-Bergmann *et al.*, 2014). Spindles in intact epithelia may also respond to other contextual clues, such as tricellular junctions (see *Discussion*).

How is symmetric spindle positioning achieved in intact epithelia (i.e., epithelial layers within or obtained from intact animals)? At the molecular level, adapter proteins such as LGN or NuMA direct recruitment of the microtubule motor protein dynein to particular regions of the cortex (including cell–cell junctions), where it (cortical dynein) helps position the spindle by pulling on the astral microtubules (Morin *et al.*, 2007; Peyre *et al.*, 2011; Bergstralh *et al.*, 2013; Bosveld *et al.*, 2016). Adapter proteins and dynein also participate in spindle positioning in isolated epithelial cells grown on patterned substrates (e.g., L-shaped fibronectin), a manipulation that promotes planar spindle orientation (Kiyomitsu and Cheeseman, 2012), and in asymmetric cell division in some systems (Siller *et al.*, 2006; Wang *et al.*, 2011), suggesting that the same players may be differentially deployed in different contexts.

In addition to dynein, spindle positioning may rely on myosin-10 (Myo10), an actin-based motor that binds to microtubules (Berg *et al.*, 2000; Weber *et al.*, 2004; Hirano *et al.*, 2011). Loss of Myo10 in *Xenopus* embryonic epithelia results in abnormalities spindle positioning (Woolner *et al.*, 2008; Woolner and Papalopulu, 2012). That Myo10 may be generally used in spindle positioning is suggested by its participation in spindle positioning in epithelial cells cultured on patterned substrates (Toyoshima and Nishida, 2007; Kwon *et al.*, 2015).

Just as important as the molecules is spindle dynamics. That is, rather than simply being assembled in the right place and orientation necessary to direct symmetric division, epithelial spindles commonly only achieve their final anaphase position and orientation well after assembly. Although there have been relatively few live-cell imaging studies of spindle dynamics during symmetric cell divisions within intact epithelia (see also *Discussion*), three general features have been observed in most of them. First, a surprising amount of spindle motility is often evident between metaphase and anaphase, with spindles undergoing a variety of rotational movements (e.g., Adams, 1996; Haydar *et al.*, 2003; Woolner *et al.*, 2008; Peyre *et al.*, 2011). Second, in those cases in which the spindle assembles in a nonplanar orientation, a rotation in *Z* occurs after metaphase onset, thereby establishing planar orientation (e.g., Roszko *et al.*, 2006; Peyre *et al.*, 2011; Bergstralh *et al.*, 2016). Third, in cases in which the spindle assembles such that it is not parallel to the long axis of the cell, a rotation in *X* and *Y* occurs after metaphase onset that may orient the spindle parallel to the long axis of the cell (e.g., Adams, 1996; Gibson *et al.*, 2011; Campinho *et al.*, 2013; Bosveld *et al.*, 2016; but see also Gong *et al.*, 2004, and *Discussion*).

The aforementioned studies and observations represent critically important first steps in characterization of epithelial spindle motility. However, because most of these studies had low temporal resolution (with time points of 1–5 min) and did not combine spindle markers with those for the cell cortex, it was not possible to answer several fundamental questions about epithelial cell spindle dynamics. For example, what, exactly, do the *XY* spindle rotations represent? Are they of a consistent magnitude and duration? Are they random, or do they make material contributions to spindle positioning; if so, how? What balances the cortical pulling forces on the spindle? How are the various motilities related to each other and to important cell cycle transitions?

To address directly and systematically these and other questions related to epithelial spindle dynamics, an imaging regime with high spatiotemporal resolution is required, as is a methodology that permits objective and quantitative characterization of mitotic spindle dynamics in the context of an intact tissue. Here we develop an automated spindle-tracking system—the "Spindlometer"—and applied it to characterize spindle dynamics in epithelia of *Xenopus laevis* embryos. This approach reveals that soon after metaphase onset, epithelial spindles undergo a series of stereotyped movements that are linked to achievement of proper spindle orientation, spindle position, and, potentially, the metaphase–anaphase decision.

RESULTS

Epithelial metaphase spindles are highly dynamic

Mitotic spindles are highly dynamic within the embryonic epithelium of the *X. laevis* gastrula animal cap. Visualized by confocal imaging of enhanced green fluorescent protein (eGFP)–tagged tubulin, the mitotic spindle moves dramatically through mitosis (Figure 1A; Woolner *et al.*, 2008). A two-probe imaging regime with both fluorescent tubulin and fluorescent histone H2B reveals fields of asynchronous epithelial cells across the animal cap (Figure 1B) and permits visualization of both spindle dynamics and mitotic transitions (Figure 1C). The first of these transitions is nuclear envelope breakdown (NEB), which is visualized by the influx of tubulin into the space previously occupied by histone signal alone (Figure 1, C and D); the next is metaphase, which is visualized by alignment of the condensed sister chromatids on the metaphase plate (Figure 1C); the last is anaphase A, which is visualized as the coordinated separation of the condensed sister chromatids (Figure 1, C and D). In this system, anaphase A onset occurs before and is easier to visualize than anaphase B (revealed by persistent elongation of the mitotic spindle). Dual-label imaging indicated that the most dramatic spindle movements occurred soon before anaphase onset (Figure 1, C and D). That is, if assembling spindles and early metaphase spindles move, it is typically orderly and directed. In contrast, upon reaching mid-metaphase, spindles displayed vigorous motion in the *XY*-plane, a behavior that is obvious in movies (Supplemental Movie S1) and kymographs (Figure 1D). These movements tapered off rapidly after anaphase onset (Supplemental Movie S1 and Figure 1D).

Spindle dynamics versus spindle location

We next sought to track spindle movements with respect to cell boundaries. Whereas tubulin is sufficient to visualize cortical microtubules in nonmitotic cells, cortical tubulin signal is lost in mitotic cells (Figure 2, A–D). We therefore used mTagBFP (Subach *et al.*, 2008) endowed with a CAAX domain (Willumsen and Christensen, 1984; Clarke *et al.*, 1988; Hancock *et al.*, 1989) to target it to the plasma membrane, which provided a stable, high-contrast label of cell edges in both interphase and mitotic cells (Figure 2, A–D).

With a probe set established for cell edge and spindle visualization, we next optimized imaging parameters to allow for sufficient capture of the predominant mitotic spindle dynamics while minimizing phototoxicity and photobleaching. Because it is established that spindles in the *Xenopus* system typically form parallel to the plane of the epithelium (Strauss *et al.*, 2006; Woolner and Papalopulu, 2012; see also Supplemental Movies S2 and S3), we used single-plane imaging. Other empirical and theoretical considerations demonstrated that three-channel, single–optical plane imaging at 5-s intervals provided the ideal balance between speed and epithelial cell health (see *Materials and Methods*).

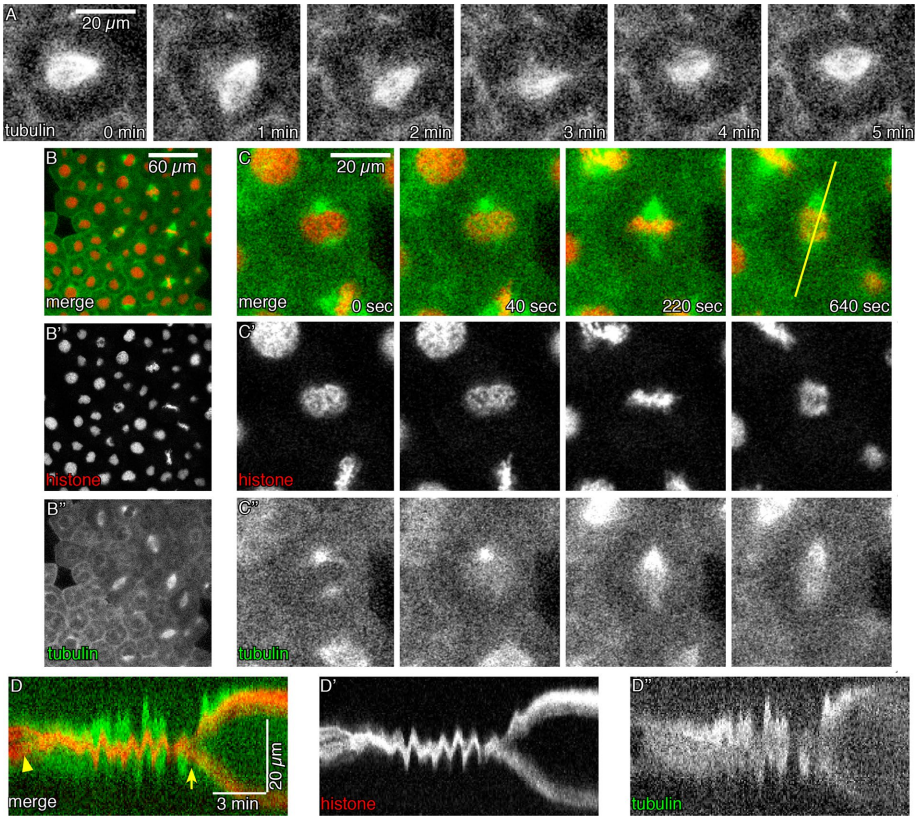

FIGURE 1: Tubulin and histone highlight mitotic landmarks. (A) eGFP–α-tubulin (GFP-Tub) highlights the highly dynamic mitotic spindle in the *X. laevis* embryo. (B) *X. laevis* gastrula animal caps contain a field of asynchronous epithelial cells, visualized with mCherry-histone H2B (mChe-H2B; B′) and GFP-Tub (B″). (C) Mitotic temporal landmarks are apparent in cells expressing mChe-H2B and GFP-Tub, including NEB (frames 1 and 2), formation of the metaphase plate (frame 3), and segregation of chromosomes in anaphase (frame 4). The line in frame 4 through the spindle poles at anaphase onset was used to generate a kymograph (D), highlighting NEB (arrowhead), anaphase onset (arrow), and spindle movements in preanaphase period.

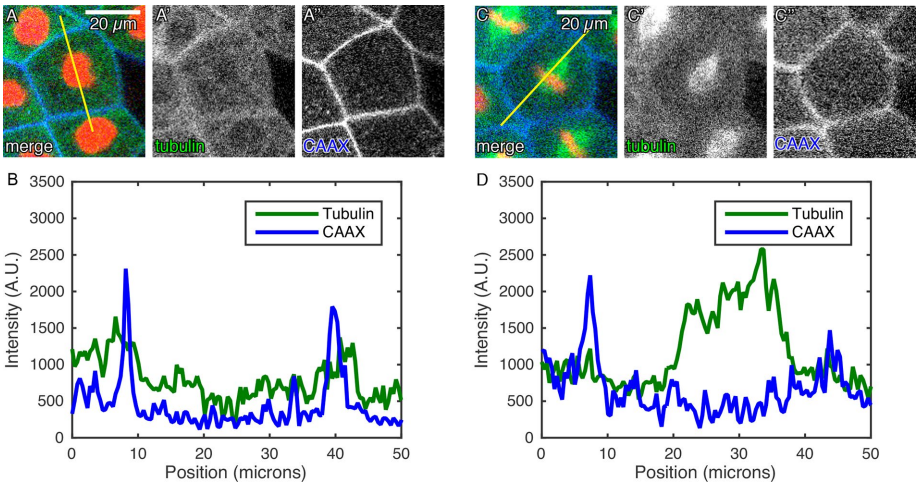

FIGURE 2: CAAX provides a bright cell-edge marker. (A) Comparison of cortical tubulin and mTagBFP-CAAX (BFP-CAAX, a membrane marker) in interphase cell with accompanying line scan (B) reveals both tubulin and CAAX signal at the cell edge. (C) Comparison of tubulin and membrane probes in mitotic cell with accompanying line scan (D) demonstrates loss of cortical tubulin in mitosis. Cells were labeled through expression of GFP-Tub, mChe-H2B, and BFP-CAAX.

After collection, three-channel time series were separated into single cell regions of interest (ROIs) in FIJI (Schindelin *et al.*, 2012), noting apparent times of NEB, metaphase, and anaphase. The orientation of the mitotic spindle was also noted and compared with the long axis of the cell at anaphase onset. This analysis showed that spindles are typically aligned with the long axis of the cell at anaphase onset, whereas centrosomes at NEB are not (Figure 3, A–C). To determine when and how spindles achieve this orientation, we manually tracked centrosome and spindle pole locations from before NEB to after anaphase onset in a MatLab graphical user interface (GUI) built specifically for this purpose (see the Supplemental Methods). Figure 3, D and E, shows a representative time series: after NEB, and accentuated at the onset of metaphase, the spindle undergoes a relatively slow, steady rotation that results in approximate alignment with the long axis of the cell (Figure 3, D and E; 200–400 s). This rotation is followed by a series of relatively rapid rotary oscillations that begin to subside shortly before anaphase onset (Figure D, 400–550 s, and E, 400–600 s). The oscillations, while more dramatic than the initial rotation, do not necessarily produce a net change in spindle orientation. As a consequence, the large magnitude of the oscillations typically overrotates the spindle past its final orientation at anaphase onset (Figure 3E). The stereotyped nature of this orientating process is made clear when rotational traces, normalized to an orientation of zero at metaphase, are averaged (Figure 3F)

The extent of the initial spindle rotation varied according to the degree to which the initial spindle orientation (i.e., the orientation of the spindle immediately after assembly) differed from its final orientation. That is, some spindles assembled with the spindle already nearly aligned in the same orientation attained at anaphase; these displayed very little initial rotation. In contrast, the occurrence of fast oscillations was a feature of spindle dynamics in all cells. For 28 manually analyzed spindles, orientation normalized to spindle orientation at anaphase onset was plotted (Figure 3G) and, of note, all spindles appeared to undergo rotational oscillations before anaphase onset, regardless of the extent of net rotation from NEB to anaphase onset. To assess explicitly whether oscillations vary with net rotation, we sorted spindles into prealigned (<35° net rotation) and nonaligned (>35° net rotation) groups. No significant difference in mitotic duration (Figure 3H), total number of oscillations (Figure 3I), oscillation amplitude (Figure 3J),

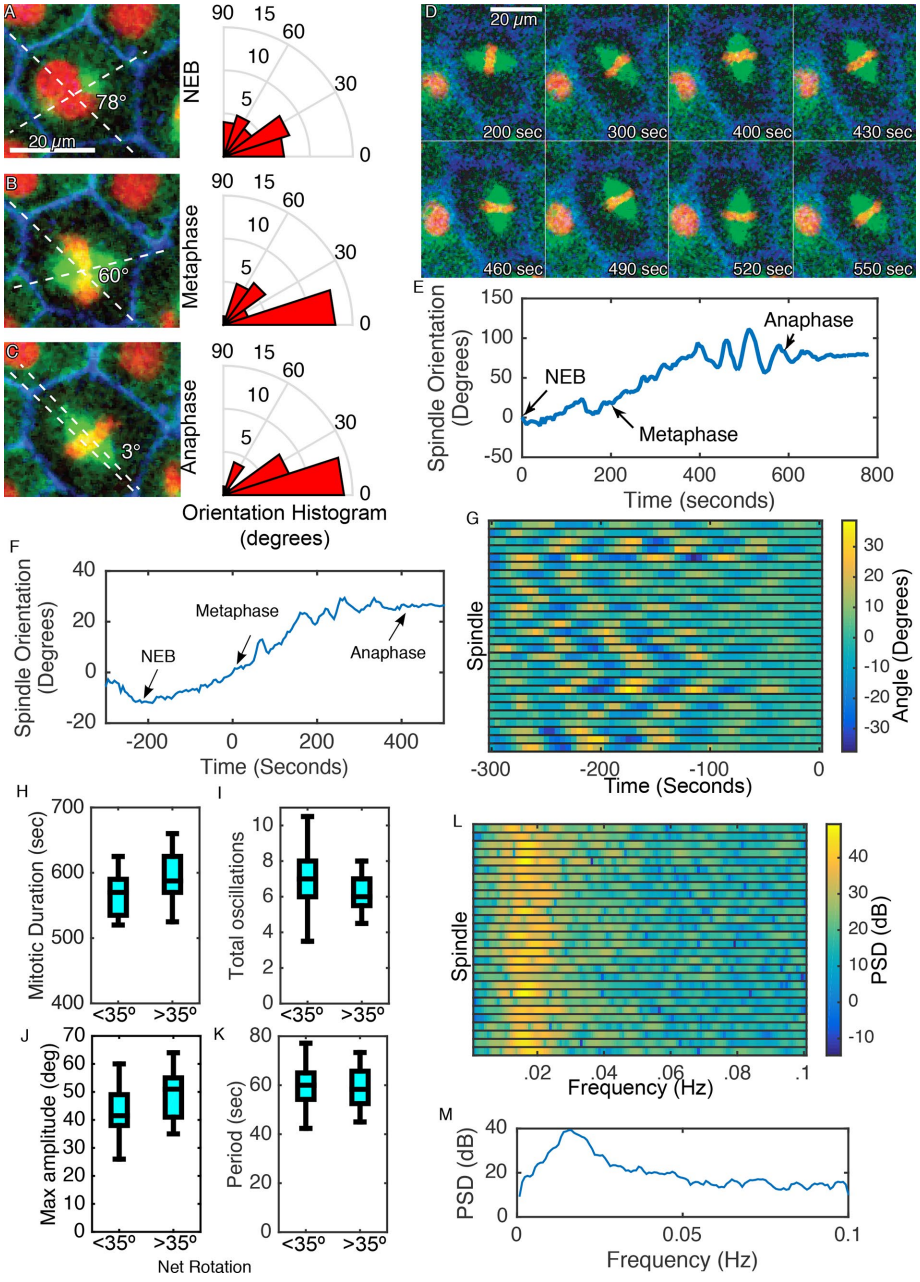

FIGURE 3: Mitotic spindles display stereotyped alignment and oscillatory rotational dynamics. The angle between centrosomes/spindle poles and the long axis of the cell at anaphase was measured in 28 cells at (A) NEB, (B) metaphase, and (C) anaphase in cells expressing BFP-CAAX, GFP-Tub, and mChe-H2B. (D) Mitotic spindles display dynamic movement, featuring preanaphase oscillations when spindle orientation is plotted (E). (F) Average spindle orientation over time for 28 manually analyzed spindles. Time 0 indicates approximate time of metaphase plate formation. (G) Twenty-eight spindles all demonstrate rotational oscillations before anaphase onset (time 0). Spindles grouped by net rotation between NEB and anaphase onset show no significant difference in (H) mitotic duration, (I) total oscillations, (J) maximum amplitude of oscillation, or (K) periodicity of oscillation. (L) Power spectral density of corresponding spindle traces from G, indicating the oscillatory frequency of each spindle. (M) Average of PSDs from L, indicating a dominant oscillatory frequency of 0.01562 Hz (period of 64 s).

and oscillatory period (Figure 3K) was found. To further characterize the nature of the oscillations, the power spectral density (PSD), a measure of oscillatory frequency in a signal, was calculated for each spindle (Figure 3L) and averaged (Figure 3M), demonstrating a dominant underlying frequency of 0.01562 Hz, corresponding to a periodicity of 64.0 s.

This analysis revealed two additional, and curious, features of the metaphase spindle "dance." First, the average maximum amplitude of oscillation in the prealigned group was >35°, indicating that these spindles undergo oscillations that are greater in magnitude than their net travel. Second, the oscillatory extrema frequently resulted in close contacts and withdrawals between the spindle pole and the cell cortex. In fact, 25 of 27 spindles had cortical contacts and withdrawals at both poles at some point during metaphase, defined at a distance of ≤7 μm as measured manually in FIJI. Intriguingly, the two spindles that did not follow the same pattern of contact and withdrawal were also the two with the longest mitotic duration. Thus we decided that further analysis should capture both the oscillatory spindle dynamics and any potential interactions between the spindle and the cortex.

Development of automated spindle-tracking software

Manual analysis of spindle orientation is prohibitively time consuming: even with the aid of the custom GUI, annotation of the pole positions of a single mitotic spindle, from NEB to anaphase, requires 30–60 min, not including measurements between the spindle poles and cell edge. Further, such analysis is inherently subjective because it relies on the observer identifying temporal landmarks (e.g., NEB) and the locations of particular structures (e.g., spindle poles) rather than the application of strict quantitative criteria. Thus we sought to develop an automated system for spindle tracking and analysis.

To accurately capture spindle dynamics within a cell, we developed a software package in MatLab, the Spindlometer, to facilitate and improve the accuracy of spindle movement analysis (see *Materials and Methods* for full details). Briefly, the user loads a time series into a custom-built user interface and selects the cell outline, spindle, and chromosome locations on a single frame. The program then refines and propagates the cell outline to all movie frames by tracing the brightest path around the cell (based on membrane probe). The spindle is tracked within each frame based on the spindle position in the previously analyzed frame and morphological filtering of tubulin signal. Spindle pole locations are determined as the extrema of the ellipse of best-fit spindle tubulin signal. Chromosomes are tracked based on the location of chromosomes in the previously analyzed frame, as well as on morphological filtering of histone signal, providing the distinct advantage of identifying aligned and unaligned chromosomes. Mitotic stage is determined based on chromosome morphology.

Dynamic features of spindle orientation

We first used the Spindlometer to determine whether the basic features of spindle dynamics identified by manual tracking (see earlier discussion) were also identified by the program and then used the program to extend the analysis of spindle dynamics to a larger data set. As seen in a time series with accompanying segmentation regions (Figure 4A; see also Supplemental Movies S4 and S5), the Spindlometer is capable of accurately recognizing and tracking cell outlines, spindles, and chromosomes through mitosis. Manually annotated (Figure 4B) and automatically calculated plots of spindle orientation (Figure 4C) show almost identical spindle rotational trajectories, indicating that the Spindlometer is indeed capable of reproducing manual analysis. Further, the timing of these events was identical, with the initial rotation beginning after NEB and the oscillations beginning to dampen shortly before anaphase onset (Figure 4, B and C). The Spindlometer detected this same pattern of events in 104 of 106 cells, with the only variation stemming from the degree to which spindles were prealigned upon assembly, which, as observed in the manual analysis, decreased the net initial rotation. The Spindlometer also detected that, in many cases, low-amplitude rotational oscillations appear to underlie the directed rotation, starting approximately at metaphase onset.

When 100 automatically generated traces were averaged (Figure 5A), net rotation was apparent throughout mitosis. However, the net rotation during the presumptive oscillatory phase remained minimal relative to the gross rotation during oscillation. The biphasic (constant rotation followed by oscillation) nature of rotational movement is clear on examination of individual rotational traces (Figure 5B). Although it is difficult to computationally divide the oscillatory regime from the constant regime, the general pattern can be described by examining the root mean square error (RMS) of acceleration of spindle rotation (Figure 5C). In an averaged trace of normalized RMS from 100 metaphase spindles, RMS is initially low, indicating constant movement, and eventually plateaus, indicating a preanaphase period of stable oscillations. This biphasic nature is more clearly seen in two sample RMS traces (Figure 5C, inset).

We next used the Spindlometer to test the hypothesis that the spindle orientation (and thus the division plane) ultimately chosen reflects alignment of the spindle along the long axis of the cell, as suggested by manual analysis, as well as work from other studies, dating to 1884 (Hertwig, 1884; O'Connell and Wang, 2000; Strauss *et al.*, 2006). This hypothesis predicts that the final spindle orientation should be parallel to the long axis of the ellipse identified by the Spindlometer. Consistent with this prediction, the long axis of the cell outline ellipse was parallel to the final spindle orientation (median misalignment <15°, $n = 100$) and thus perpendicular to the ultimate division plane regardless of whether the ellipse measurement was made at NEB, metaphase, or anaphase ($p = 0.99$; analysis of variance $F(5, 610) = 0.03$).

Spindle orientation and dynamics can be considered in terms of both extrinsic factors such as cell morphology and intrinsic factors such as spindle movements, both of which were assessed in detail using the Spindlometer. With respect to cell morphology, the angle between spindle long axis and cell long axis versus cell eccentricity was plotted and fitted with a linear regression model, revealing that angle decreases as eccentricity increases (Figure 6A, slope = –59.6, $p < 0.0001$), as expected if the spindle is selecting the long axis for alignment. To determine whether changes in eccentricity during mitosis might actually be responsible for the observed changes in spindle orientation, we compared the cell eccentricity at NEB versus anaphase. We observed a decrease (Figure 6B, $p < 0.0001$, paired t test), indicating that, on average, cells become rounder as mitosis progresses. However, no significant linear trend is observed when angle is compared with change in eccentricity (Figure 6C, $p = 0.24$),

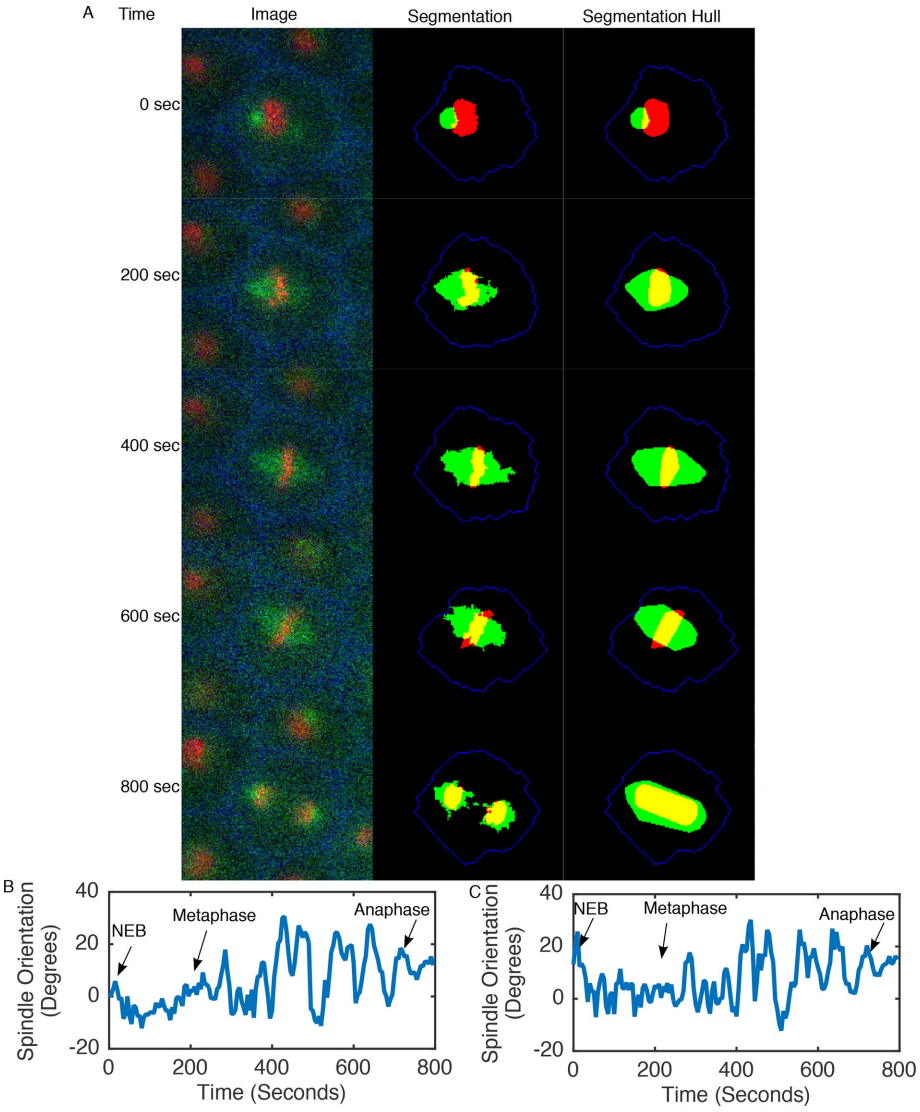

FIGURE 4: Automated analysis detects spindle rotational oscillations. (A) A time series of mitosis in cells expressing mChe-H2B, GFP-Tub, and BFP-CAAX (left), with accompanying automatically recognized regions (middle) and the convex hull of those regions (right), output from the Spindlometer. (B) Manually and (C) automatically calculated plots of spindle rotation demonstrate rotational oscillations before anaphase onset.

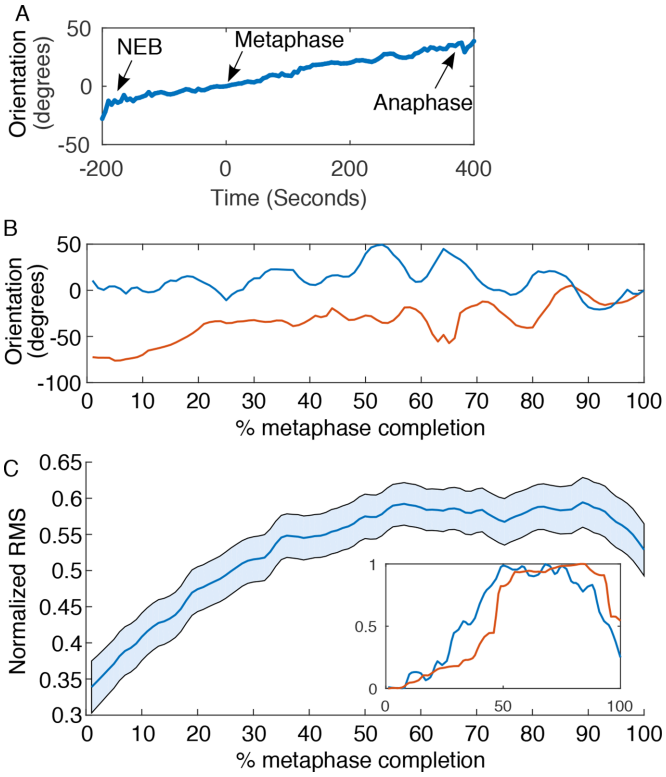

FIGURE 5: Analysis of oscillations reveals biphasic movement. (A) Average of 100 rotational trajectories reveals net rotation through mitosis, with slight apparent oscillation and decrease in net rotation toward anaphase onset. (B) Rotational traces of two spindles, one that is prealigned with the anaphase axis and one that is not. (C) Average normalized RMS of spindle rotational acceleration over 2-min intervals (24 frames) of 100 spindles during metaphase. This metric will be 0 if the spindle is still or has a constant rotational velocity and increases with greater changes in velocity over the 2-min intervals. RMS is low at early time points and steadily increases to a plateau, indicating that rotational velocity is more constant in early metaphase, consistent with a rotational but nonoscillatory regime, followed by a period of more tumultuous acceleration, indicative of oscillation. Inset, sample RMS traces corresponding to the rotational traces in B.

indicating that such changes are unlikely to contribute to changes in spindle orientation.

With respect to spindle movements, the Spindlometer was used to track spindle positioning in *X* and *Y*, based on the rationale that consistent generation of equal-sized daughter cells by an epithelium implies that the spindle be close to the approximate middle of the cell in *X* and *Y* when anaphase occurs. To accomplish *XY*-tracking, we calculated the distance between the cell centroid and histone region centroid at all image frames in metaphase and then compared the average distance between centroids to the distance between centroids at anaphase onset. This analysis demonstrated that spindles are significantly more centered ($p = 0.0004$, paired *t* test, $n = 100$) at anaphase onset than during the rest of mitosis (Figure 6D).

Spindle oscillations

We next used the Spindlometer to characterize in detail the remarkable rotary oscillations that consistently preceded anaphase. The power spectral density for 100 spindles was calculated in the 150 s before anaphase onset and averaged, revealing a peak at 0.01953 Hz (Figure 7A). This corresponds to an oscillatory period of 67.4 s, very similar to the peak seen in manually analyzed traces (Figure 3M).

We next performed a mean square displacement (MSD) analysis of all metaphase spindle pole locations to determine whether points behave in a restricted, diffusive, or directed manner (Figure 7B). Not surprisingly, it appears that spindle poles exhibit directed behavior at small time lags, demonstrated by the initial upward curvature of the MSD trace. However, the MSD traces also indicate that the spindle poles exhibit restricted behavior at longer time lags, indicated by the leveling out of the trace, presumably a result of their oscillatory movement and spatial restriction in the cell.

Spindle pole velocities were reconstructed in a spindle-based moving reference frame to highlight the rotational oscillations (Figure 7C). Not surprisingly, cross-correlation analysis showed strong correlation in the radial component at zero time lag, indicating that both spindle poles typically rotate in the same direction (Figure 7D). The magnitude of this correlation may be of interest in future studies of force balance on the mitotic spindle, as it could be used in the evaluation of the relative forces simultaneously acting on the spindle poles. Of interest, the outlying peaks in the average cross-correlation have maxima at ±50 s, corresponding roughly to the frequency of the oscillations.

Cortical contacts

Finally, we applied the Spindlometer to analysis of the "touching" behavior seen in manually analyzed samples, in which spindle poles closely approach the cortex during the oscillatory phase of spindle dynamics. To explore the interactions between the spindle poles and cell cortex, we calculated velocities of idealized spindle poles (see the Supplemental Methods) along (radial) and perpendicular to (axial) the cell boundary. We then plotted velocity against distance to the cell edge and calculated least-squares linear fits (Figure 8A). Analysis of covariance of the fitted lines reveals that radial velocity is greater than both negative and positive axial velocity components at the *Y*-intercept, a proxy of cell edge ($p < 10e\text{-}10$ for both; multiple-comparison posttest), suggesting that radial spindle movements dominate, especially near the cortex. Of interest, the positive component of axial velocity is greater than the negative component ($p = 0.0002$; multiple-comparison posttest), implying that the spindle moves away from the cortex more quickly than it is drawn in. The slope of the axial component fits was not significantly different ($p = 0.23$), whereas the slope of the radial velocity fit was significantly less than both positive and negative axial components ($p < 10e\text{-}10$ for both, multiple-comparison posttest). This implies that, as the pole distance increases from the cortex, the radial and axial forces are relatively balanced.

To investigate the relationship between cortical contact events and anaphase onset, we calculated the times of all cortical contacts during metaphase. A cortical contact was defined as when a spindle pole moves within 7 μm of the cell boundary with a prominence of at least 1.5 μm (Figure 8B). Of 100 spindles analyzed, 97 displayed contact by at least one pole, and 78 of 100 spindles had cortical contact by both poles. For these spindles, a trace of average pole distance to cell edge versus anaphase onset (Figure 8C) demonstrates a decrease preanaphase, overlapping with the approximate time frame in which oscillations dominate. Plots of the times of closest cortical proximity (Figure 8D) show a steady increase in cortical contact through metaphase. A commensurate increase in discrete cortical contact events was also observed in this time frame (Figure 8E), confirming that oscillations indeed lead to increased cortical contact.

The foregoing results prompted us to examine the cortical contact behavior of the mitotic spindle relative to its final (i.e., anaphase)

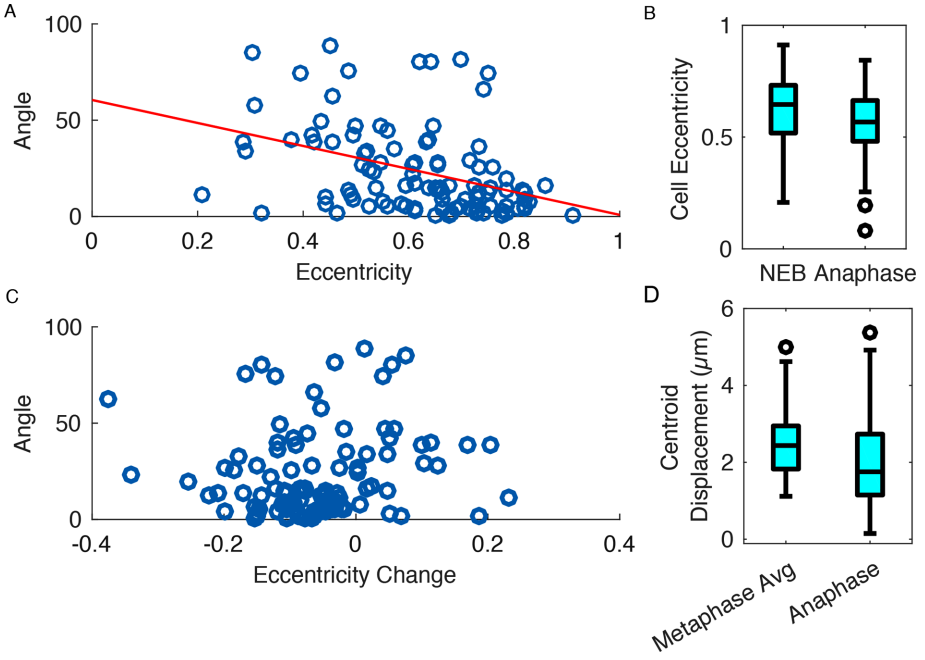

FIGURE 6: Comparison of cell and anaphase spindle metrics. One hundred cells expressing mChe-H2B, GFP-Tub, and BFP-CAAX were analyzed with the Spindlometer. (A) Comparison of angle between anaphase spindle orientation and NEB cell orientation and cell eccentricity reveals decreased angle as cell eccentricity increases (linear regression fit, slope = –59.6, $p < 0.0001$). (B) Average cell eccentricity decreased through mitosis ($p < 0.0001$, paired t test). (C) Angle between spindle and cell orientation is independent of change in cell eccentricity through mitosis ($p = 0.24$). (D) Comparison of distance between spindle centroid and cell centroid during metaphase and at anaphase onset reveals a significant decrease of displacement (increased spindle centering) at anaphase onset ($p = 0.0004$, paired t test).

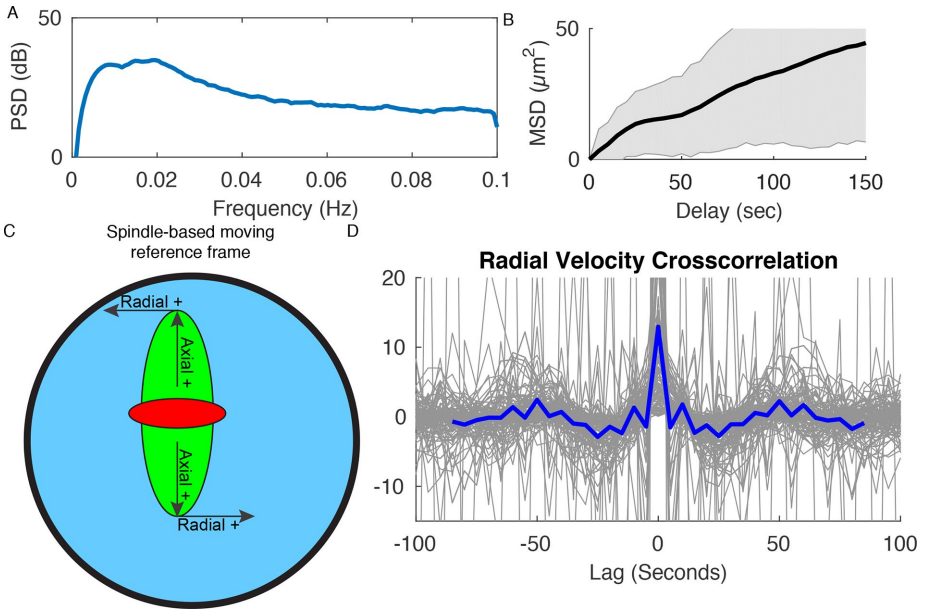

FIGURE 7: Analysis of spindle pole movements. (A) Averaged power spectral density of 100 automatically calculated spindle rotational trajectories in the 150 s before anaphase onset reveals a similar maximum to that seen in manually analyzed spindles. (B) Mean square displacement of 200 metaphase spindle pole locations reveals an initial supralinear (directed) behavior and later infralinear (restricted) behavior. Black line represents mean MSD; gray areas indicates SD. (C) Diagram of spindle-based moving reference frame used to highlight spindle dynamics. Cross-correlation of radial velocity components (D) demonstrates correlated movement at zero time lag, as well as outlying peaks (–50 and 50 s) indicative of oscillation.

orientation. To do this, we measured the distance from the spindle poles to the points on the cell boundary along the line through the cell centroid positioned at the anaphase spindle orientation (Supplemental Figure S4D). This measurement can be used to determine whether the spindle poles contact a specific target at the cortex along its (the spindle's) final orientation. From this measurement, it is clear that the spindle steadily approaches this point during mitosis (Figure 8F). Cortical contact at this point was then calculated, again at a threshold of 7 μm, but this time with a prominence of 3 μm. Strikingly, a peak of cortical contact was seen in the range ~35–65 s before anaphase onset (Figure 8G). Coupled with the following drop in cortical contacts, this measurement indicates that most spindles have a final cortical contact that is in line with their final orientation, followed by a withdrawal from the cortex, presumably as the spindle nears the center of the cell, as seen in Figure 6D. In contrast, there was an apparent peak of contact with off-target cortical sites in mid-metaphase, declining before anaphase onset (Figure 8H).

DISCUSSION

To enable study of the dynamics and mechanics controlling mitotic spindle positioning, we set out to define an imaging protocol and develop an imaging analysis pipeline for the study of spindle dynamics. Other systems have been described for automated spindle motility analysis that rely on differential interference contrast images for cell detection and provide basic measurements of spindle positions in single cells or early *Caenorhabditis elegans* divisions (Corrigan *et al.*, 2013; Cluet *et al.*, 2014). The software developed here—the Spindlometer—provides a useful counterpart to those systems, in that it permits cell outline detection in fluorescence images (which will make it useful well beyond the current application), provides direct measurements between the spindle and the cortex, and incorporates strict quantitative criteria for mitotic stage determination. The Spindlometer can recapitulate results of manual analysis with minimal user input. Of greater importance, the power of the automated region recognition far exceeds that of manual analysis. Once regions are designated, it is possible to make measurements that would be unreliable or nearly impossible to make otherwise. Here we use it to reveal unexpected features of mitosis in unmanipulated epithelial cells (see later discussion). However, it will be also be of considerable interest to compare spindle dynamics in

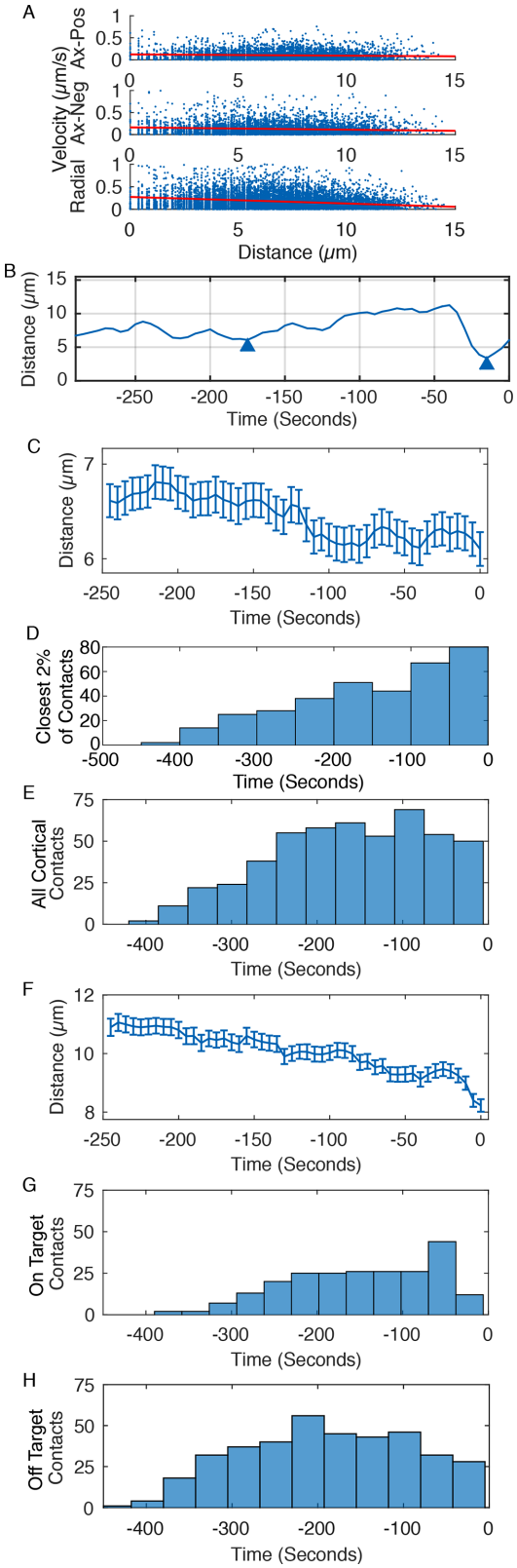

FIGURE 8: Measurement of spindle–cortex interactions. For 100 spindles analyzed with the Spindlometer, spindle pole velocity was broken down into components parallel to (radial) or perpendicular to (axial) the nearest point on the cell boundary. (A) Linear fits to positive axial velocity, negative axial velocity, and nondirectional radial velocity against distance to cell boundary. Radial velocity is significantly greater than either axial component at the cell edge ($p < 0.001$). Negative axial velocity is significantly greater than positive axial velocity at the cell edge ($p < 0.001$). (B) Sample trace of distance between spindle pole and cell boundary. Triangles denote troughs where distance drops to <7 μm. C) Average distance of 200 spindle poles to cell boundary during metaphase. Time 0, anaphase onset. Error bars, SE. (D) For 200 metaphase spindle poles, histogram indicating the 2% of time points at which each pole was closest to the cortex, indicating a general increase in cortical contact through metaphase. (E) Timing of cortical contacts for 100 spindles during metaphase. A contact is constituted by proximity within 7 μm of the cell boundary followed by withdrawal by at least 2 μm. (F) For 200 spindle poles, average distance between the spindle pole and points on the cell cortex that fall along the anaphase axis. Time 0, anaphase onset. Error bars, SE. (G) Timing of on-target cortical contacts at the points on the cortex along the anaphase axis. Contact is constituted by proximity within 7 μm, followed by withdrawal of at least 3 μm. (H) Timing of off-target (unaligned) cortical contacts. Cortical contacts as defined in D were sorted to include only those that occurred at least 9.3 μm from the target point defined in G.

control cells versus those subject to different manipulations. As our understanding of the complex mechanisms controlling spindle positioning and orientation grows, we anticipate that detection of subtle dynamic phenotypes will be necessary; the Spindlometer provides the means for such detection.

Two other features of the Spindlometer deserve comment. First, although it was developed specifically for use in *X. laevis* embryos, it can be used in nearly any system in which a brightest-path method of cell detection is valid. Given that the prenylated fluorescent proteins are broadly useful as simple, high-contrast markers of the plasma membrane, this is not a difficult requirement to satisfy. Second, the program is structured in such a way that other boundary detection methods could be swapped in with minimal modification. Similarly, other forms of spindle analysis (e.g., those based on spindle morphology; Grenfell *et al.*, 2016) could certainly be used in conjunction with our segmentation techniques.

The Spindlometer allows for accurate tracking of spindle movements, as well as measurement of distances between spindle and cell boundary. Although methods exist for tracking spindle position by specific centrosome or pole markers (Decarreau *et al.*, 2014), our whole-spindle tracking method has the advantage of detecting the entire spindle, enabling more intricate analysis of spindle position and morphology. Further, although our method was developed mainly to track the position of the spindle in the image (*XY*) plane, it is more robust to movements in the *Z*-plane than methods that track spindles by centrosome/pole markers, which are prone to going out of focus.

The mitotic spindles in *X. laevis* embryo epithelia typically assemble parallel to the *XY*- plane (Strauss *et al.*, 2006; Woolner and Paplopulu, 2012; Supplemental Material), consistent with theoretical models that demonstrate that spindle orientation is innately biased toward this plane (Jüschke *et al.*, 2014). However, in models or situations in which movement in the *Z*-plane is greater, the Spindlometer is capable of accepting *Z*-projections or, if desired, tilt in the *Z*-axis could be estimated in single-plane images as a function of the relative sizes of the hemispindles. Further, in circumstances in which tilt is great in single-plane images (large difference in hemispindle size), some measurements from the Spindlometer, such as chromosome centroid, will be robust to tilt-induced error. Thus, when applying the Spindlometer to other systems, outcome measures can be specifically selected based on the usual dynamics of the system.

The *XY* spindle movements described here are clearly not peculiar to the frog system but instead reflect a general feature of intact epithelia in a variety of contexts. For example, studies of intact epithelia in flies (Bergstralh *et al.*, 2016), chicks (Peyre *et al.*, 2011), and rodents (Adams, 1996; Haydar *et al.*, 2003) revealed that mitotic spindles can undergo extensive *XY* movements before anaphase, similar to the findings here and our previous work (Woolner *et al.*, 2008). What was not apparent in previous studies (including our own) was the extent to which these movements are stereotyped, a finding made possible by the development and application of the Spindlometer. Essentially, we find that after achieving metaphase, the spindle undergoes a consistent, two-part dance. The first part is dominated by a comparatively slow and progressive rotation that continues until the spindle achieves an orientation that is within ~10° of its final orientation (i.e., the orientation it will have at anaphase). The extent of the rotation is dictated by the orientation of the spindle at metaphase onset: if the spindle is relatively close to the final orientation, the rotation is relatively short; if the spindle is relatively far from the final orientation, the rotation is relatively long.

The second part of the dance is dominated by a series of comparatively fast spindle oscillations that, at first glance, do not seem terribly useful. That is, by the time the oscillations begin to slow just before anaphase onset, the net orientation of the spindle is more or less equivalent to where it was before oscillation onset. However, these oscillations are accompanied by close approach of the spindle poles to the cortex, a dance step that we propose later might be very useful indeed. In any case, the results presented here make it abundantly clear that metaphase onset does not represent the end of spindle motility, as in the textbook view of mitosis, but the beginning, at least within the intact vertebrate epithelium.

To what extent does the frog spindle dance mimic the dynamics of spindles described in other intact epithelium models? Because most of the other studies were conducted at much lower temporal resolution, it is hard to be sure. However, the results of Peyre *et al.* (2011) obtained with chick showed a transition in spindle velocity between early and late metaphase that is consistent with our findings of two different regimes of *XY* motility (Peyre *et al.*, 2011; Figure 1G). Although they ultimately concluded that the *XY* rotations were random, this likely reflects the fact that they did not have the benefit of a plasma membrane marker and used 2-min sampling intervals. Similarly, in an earlier study of spindle orientation in *Xenopus* embryos, which concluded that metaphase spindle rotations do not contribute to spindle alignment (Strauss *et al.*, 2006), a 1-min sampling interval was used, and no plasma membrane marker was used. Both of these conditions would have made it difficult to reliably detect and track the alignment of the spindles along the long axis of the cell during the first part of the dance, as well as the rapid oscillations and touching behavior characteristic of the second part of the dance. Rotational oscillations of metaphase spindles were also observed by Adams (1996) in studying symmetric cell division in rat neuroepithelial brain slices. Although the longer sampling interval (30 s) and lack of a plasma membrane marker make it difficult to compare to the present results, Adams (1996) reported that the rotations were not random and had the net effect of orienting the spindle on its ultimate division axis relative to the beginning of metaphase.

What powers the metaphase spindle dance? In other systems, cortically localized dynein is believed to drive spindle movements during spindle assembly (e.g., Peyre *et al.*, 2011; Kiyomitsu and Cheeseman, 2012; Kotak *et al.*, 2012) and after anaphase onset (O'Connell and Wang, 2000; Kiyomitsu and Cheeseman, 2013). Both the initial rotation of the spindle and the approach of spindle poles to the cortex during the oscillatory phase observed here are consistent with this possibility, in that cortically localized dynein is expected to result in microtubule sliding along the cortex (Adames and Cooper, 2000). Indeed, such sliding is predicted to produce greater radial spindle pole velocity than axial velocity, especially when the pole is near the cortex, exactly as observed here (e.g., Figure 7A). This observation would not have been possible without automated spindle recognition and a large data set.

The basis of the rapid movement of spindles away from the cortex is more mysterious, in part because it was not observed previously and in part because it is actually faster than the movement toward the cortex, suggesting a different basis. This motility also implies that a mechanism exists that specifically couples and uncouples the spindle from the cortex because in the absence of such a mechanism, dynein-powered pulling forces would be expected to pin the spindle to the cortex. To the best of our knowledge, the existence of such a mechanism has not been previously reported, providing further evidence of the utility of the automated analysis used here. One possible mechanism underlying this expulsion might rely on another function of cortical dynein—to capture astral microtubules and incite shrinkage (Laan *et al.*, 2012).

Finally, what is the point of the dance? Is it just something interesting that spindles in epithelia do, or does it somehow contribute to proper cell division? Although the stereotyped nature of the dance suggests that it is important, more direct evidence from the results of the automated analysis can be adduced. Most obviously, the slow rotation that dominates the first part of the dance results spindles that were initially positioned well off their final (i.e., anaphase) axis coming to within a few degrees of it. Less obvious, but just as important, the dance also brings the spindle to the approximate middle of the cell in the *XY*-plane. This behavior has not been described in any other system, likely because detection of such behavior would have been difficult without the automation and imaging approaches developed here. In any case, the significance of the centering behavior is clear: failure to center the spindle in *XY* would result in unequal-sized daughter cells, which would likely lead to disorganization of the epithelium.

The point of second part of the dance, in which the rapid oscillatory movements dominate, is much less obvious because the spindle ends up in roughly the same orientation it had when the oscillations began. However, the results obtained from the automated spindle analysis reveal three consistent features of the oscillatory spindle dynamics. First, they bring the spindle poles in close proximity to the cortex (i.e., they drive spindle-cortical touching). Second, each "touch" is followed by rapid movement of the spindle away from the cortex. Third, an increase in on-axis touching is temporally correlated with anaphase onset. Collectively these results suggest that the oscillatory movements represent a type of hypothesis testing behavior in which the spindle probes the cortex for a signal of the "ideal" location. Ideal locations would correspond to those that are on-axis such that the subsequent expulsion of the spindle from the cortex results in the spindle being in the approximate middle of the cell in *X* and *Y* upon anaphase onset. Thus, the expulsion ensures that the movement of the spindle toward the middle of the cell in *X* and *Y* from the first part of the dance is enforced. The ideal location would also reflect optimal alignment in the *XY*-plane. Because it has been shown that spindle-centering behavior continues after anaphase onset (Collins *et al.*, 2012; Kiyomitsu and Cheeseman, 2013), we consider the *XY* alignment to be the most important function of this mechanism. The signal, in turn, would be responsible for triggering the onset of anaphase. In other words, we suggest that the oscillations serve as part of a mechanism

that ensures that anaphase onset is coupled to proper spindle positioning and orientation, an idea previously proposed for budding yeast (e.g., Caydasi *et al.*, 2010; Moore *et al.*, 2010) and cultured mammalian cells (O'Connell and Wang, 2000).

This hypothesis should be considered provisional, as the target point of "on-target" touching was determined postanalysis. This was done mainly because, although the long axis of the cell is a reasonable predictor of final spindle orientation, it is far from perfect. Nonetheless, we note that there is a potential cellular and molecular difference that typifies the cortical region of on-axis touches—tricellular junctions. Tricellular junctions have been shown to harbor several different proteins not found in bicellular junctions (Ikenouchi *et al.*, 2005; Oda *et al.*, 2014) and are known to be sites of localized NuMA, a dynein-binding protein (Bosveld *et al.*, 2016). Although none of these is known to be directly involved in mitotic regulation, their existence renders plausible the notion that such regulators might be present. Regardless of how it might work, coupling spindle oscillations and cortical touching to anaphase onset would have the salubrious effect of helping the cell delay anaphase until the spindle has achieved the proper position and orientation needed for generation of equal-size daughter cells properly positioned within the plane of the epithelium.

MATERIALS AND METHODS

Plasmids and constructs

PCS2-eGFP–α-tubulin (human), PCS2-mChe-histone H2B (human), and PCS2-mChe-CAAX (as mCherry-Membrane, from human ras; Reyes *et al.*, 2014) were generated previously. PCS2-mTagBFP-CAAX was generated by PCR amplification of mTagBFP (Evrogen) with PFU Ultra DNA polymerase (Agilent) with custom DNA oligonucleotide primers (IDT) GCAGGATCCAAACCATGAGCGAGCTG and ATCTGAGTCCGGACTTGTGCCCCAGTTTGC. The PCR product was cleaned up using the Wizard SV Gel and PCR Cleanup Kit (Promega), digested with *Bam*HI and *Bsp*EI (NEB), gel purified, again cleaned up with the Wizard kit, and ligated (T4 DNA Ligase; Promega) into PCS2-mChe-CAAX that had been similarly digested to remove the mCherry-coding DNA sequence.

For generation of mRNA, all aforementioned PCS2 constructs were linearized with *Not*I or *Not*I-HF (NEB), cleaned up with the Wizard kit, and transcribed with the mMessage mMachine SP6 Transcription Kit (Ambion). The transcription product was cleaned up with the RNEasy MinElute Cleanup Kit (Qiagen), diluted to 0.5–1 g/l, aliquoted, and stored at –80°C until use.

Culture and microinjection of *X. laevis* embryos

Embryos were obtained as previously described (Woolner *et al.*, 2008). Embryos were microinjected in 2/2 blastomeres with 5 nl of water and mRNA. mRNA was prepared in dilute mixed solution of 0.015–0.3 g/l for eGFP–α-tubulin, 0.008–0.015 g/l for mChe-histone H2B, and/or 0.06–0.1 g/l for mChe-CAAX and mTagBFP-CAAX, as appropriate. Embryos were cultured overnight at 16°C (~18–22 h) before imaging.

Imaging

All imaging was performed on a three-channel point scanning confocal microscope (Prairie Technologies, now a division of Bruker) with a 60× objective (Olympus). Laser power (405, 488, and 561 nm) and photomultiplier tube voltage was adjusted to optimize image quality for each sample. Laser interlacing was used to reduce bleedthrough between channels, although the 405- and 561-nm lasers were included in the same track to reduce imaging time.

Preliminary image analysis

Image Tiff stacks were initially compiled in FIJI using the BioFormats plug-in (Linkert *et al.*, 2010). Line scan data were obtained using the Plot Profile tool. Kymographs were obtained using the stack resliced tool. Initial thresholding was performed in FIJI on median filtered images (2.5 radius), and converted into binary through the Otsu method in the Auto Threshold tool.

Image processing and data analysis

All MatLab (version R2015a; Math Works) GUIs were developed through the MatLab GUIDE. Tiff stacks were loaded into MatLab GUIs using the tiffread2 function (Nédélec *et al.*, 2001). The Spindlometer GUI is capable of accepting individual Tiff stacks for each channel or combined three-channel Tiff stacks.

In the Spindlometer GUI, image registration is achieved by translation through imregister. Translations are applied to any existing regions of interest as well as images. All plots were generated in MatLab. MSD analysis was performed using the MSDAnalyzer toolbox (Tarantino *et al.*, 2014). Cross-correlation analysis was performed using the MatLab xcorr function. Power spectral densities were calculated with the periodogram function. PSD averages were performed on dB-weighted spectra. All statistical analysis was performed in MatLab using the stated tests.

Spindlometer workflow

The core of the Spindlometer consists of two main programs—a GUI for loading images into MatLab and initializing variables used for the image segmentation subroutines described in the following sections, and the program that allows for batch processing of image data. Once an image series is loaded into the GUI, the channels can be labeled appropriately, and the channel that serves as cell outline can be selected. Individual cells within the image series are then selected, and beginning and ending points are manually selected (to minimize computational overhead in long image series with multiple mitotic events). Cell outlines are then initialized, with the only criterion that they be represented by a probe that forms a bright path around the cell (see next section). Spindles and chromosomes are also initialized, with the criterion that they be light on a dark background. The GUI can be used with any system that meets these requirements and is not specific to *Xenopus*, with the caveat that the aforementioned cellular features must be of reasonable clarity and not horribly degraded by noise.

Cell outline segmentation

The first step required development of a method for segmentation of cell outlines (i.e., conversion of cell outlines into a minimal form suitable for automated analysis). Initially, mTagBFP-CAAX grayscale images of single-cell ROIs were converted into binary images at a threshold determined by Otsu's method (Otsu, 1979; Supplemental Figure S1A). This approach proved problematic for two major reasons. First, it was not robust to intensity fluctuations around the cell boundary: when portions of the cell boundary were substantially darker than the rest of the boundary, they were lost, resulting in an open contour (arrowhead, Supplemental Figure S1A″). Second, the width of a binary outline depends on the boundary brightness of any neighboring cells, which means that the identified boundary will vary, depending on the level of mTagBFP-CAAX expressed by the neighbors of the cell of interest.

As an alternative to a threshold-based method for cell outline segmentation, we used a brightest-path approach similar to that used in MEDUSA, a program successfully used to identify and track the edges of tissue wounds in *Drosophila* (Zulueta-Coarasa

et al., 2014). To justify the use of the brightest-point approach, it was first necessary to test whether CAAX-modified fluorescent proteins provide a faithful readout for the true edge of the cell. To accomplish this, we microinjected mRNA encoding mTagBFP-CAAX mRNA into one blastomere at the two-cell stage and then microinjected mRNA encoding mChe-CAAX into the other and then, at the gastrula stage, imaged areas of interface between the two probes (Supplemental Figure S1B). Line scans of these areas revealed overlapping peaks of signal at the cell boundary, with each probe skewed toward the interior of its respective expressing cell (Supplemental Figure S1C). Near colocalization of these peaks indicates that the CAAX signal is strongest at the cell–cell interface, making a brightest-path approach ideal for defining cell outlines.

Our approach to brightest-path segmentation, although similar to the MEDUSA pipeline (Zulueta-Coarasa *et al.*, 2014), contains several key differences adapted for our system (see Supplemental Methods). The workflow is as follows. A three-channel Tiff image series is loaded into a MatLab GUI designed for ROI management, temporal landmark (e.g., NEB) annotation and, if needed, image registration (Supplemental Methods). ROIs are then selected for each cell to be analyzed, and first and last frames are selected, as is a frame for manual region annotation to initialize the automated segmentation. Once ROIs and time frames are selected, the cell outline is manually traced on a CAAX-only image (Supplemental Figure S1D). Initialization parameters, discussed later, are also established for tubulin channels and histone channels at this time. The manually drawn outline is automatically subsampled at every 20th point, and the shortest, brightest path between each point is calculated using the LiveWire (Fernandez-Gonzalez and Zallen, 2011). The resultant path is again automatically subsampled, this time at the locations halfway between the original subsampled points. The subsampled points are reconnected by the LiveWire, resulting in a shortest, brightest path around the cell. This path is constrained to the cell boundary by manual annotation but now only contains originally selected points if they are indeed part of the brightest path.

The next frame in the time series is then initialized using imregdemons, an algorithm designed for registration with local deformation. This approach was chosen over traditional registration methods (translation, rotation, stretch, and skew) because the cell outline frequently undergoes local deformation. To minimize registration errors, input images are median filtered. The registration displacement fields are then applied to the segmented outline from frame 1. This contour undergoes subsampling and refinement, just as the originally drawn outline did. This process is looped to cover all frames in the time series (Supplemental Figure S1D).

Spindle segmentation

Our initial approach to spindle segmentation involved simple thresholding to convert the tubulin image to binary (Supplemental Figure S2A). Although in some instances this was sufficient to produce a binary object that appeared to accurately represent the spindle, thresholding was not satisfactory due to its inability to cope with nonspindle tubulin signal hot spots such as remnant cortical microtubules (especially pre-NEB), astral microtubules, and scattered light from cortical microtubules of neighboring cells. The astral microtubules are particularly problematic, in that they are contiguous with the mitotic spindle and, if above threshold, are unlikely to be removed from a binary image by discarding all but the largest object, which is otherwise sufficient to remove small, discontinuous tubulin foci.

Therefore a more sophisticated filter is needed for proper segmentation of the spindle. When a line scan is taken along the long axis of a mitotic spindle with clear adjoining astral microtubules, there is a dip in signal between the spindle pole and astral microtubule signal (Supplemental Figure S2B; arrowhead). With this physical arrangement, a morphological reconstruction filter can be used to remove the astral signal. To do this, a mask containing seed points of user-defined intensity is first applied to the image. As implemented in the MatLab function imreconstruct, the filter works outward from the initial seed points, assigning neighboring pixels either the pixel value of the original image pixel or the value of the neighboring seed pixel, whichever is lower. In this way, image intensity is greatest at the seed pixels in the mask and can only decrease or remain the same as the filter works outward. Thus astral microtubules are virtually erased from the image because of the intensity dip near the spindle pole, as are other nonspindle tubulin foci. Thresholding can then be applied to identify the spindle object.

To implement the morphological reconstruction filter for spindles, the spindle/tubulin image is initialized by picking two points, preferably near the poles of a metaphase spindle. A 3-pixel-wide line connecting these points, with intensity equal to the image intensity at those points, is used as the mask for the morphological reconstruction (Supplemental Figure S2C). The morphological reconstruction is then performed on a median-filtered image of the cell, bounded by the already-segmented cell edges. A threshold is then calculated by Otsu's method, and a binary image containing the spindle object is generated. An ellipse is fitted to the convex hull of the spindle object, and a line connecting the foci of that ellipse is calculated (Supplemental Methods). Owing to the proximity of the elliptical foci to the edge of the spindle, the line is then eroded to two-thirds of its original length. Registration with local deformation is used to transfer the endpoints of the line to the next frame of the time series in the same way that it was used to transfer cell boundary points from frame to frame. A 3-pixel-wide line is then drawn between the resultant points, forming the mask for the next frame. Again, this process is repeated to cover all frames in the time series (Supplemental Figure S2C).

Chromosome segmentation

Chromosome segmentation is in some ways simpler than spindle segmentation in that, whereas both entail a bright, solid region as a target, there is far less background in the histone channel. However, the fact that chromosomes provide the information essential to identify NEB, metaphase, and anaphase imposes additional requirements on the segmentation process. Of these, identification of metaphase was most challenging, in that the segmentation must be able to distinguish between aligned and unaligned chromosomes (Supplemental Figure S3A). To accomplish this, the segmentation pipeline developed for spindles was applied directly to the histone channel, with two key differences (Supplemental Figure S3B). First, a full-length line connecting elliptical foci is used to initialize subsequent frames instead of a line of two-thirds length to ensure that chromosomes located at the far ends of the metaphase plate are detected. Second, the threshold used to create the binary version of the morphologically reconstructed histone image is also applied to the pre–morphological reconstruction image, resulting in regions that contain all histone signal, not just the chromosomes aligned at the metaphase plate. The Spindlometer also recognizes unaligned or lagging chromosomes. Specifically, when a chromosome is not properly aligned, the ratio of the area in the morphologically reconstructed region to the area in the non–morphologically reconstructed region will be significantly <1, a condition that can be tracked through the duration of mitosis to document chromosome alignment anomalies.

Elliptical fitting to determine spindle parameters

Once cell edge, spindle, and chromosome regions were determined, region parameters were extracted using the regionprops function in MatLab. Some parameters were measured directly from the region (e.g., perimeter and centroid), and others were measured from an ellipse fitted to the region (e.g., eccentricity, orientation, major axis length, and minor axis length; Supplemental Figure S4, A and B; see the Supplemental Methods for details and rationale for ellipse fitting).

Physical distances were also measured between segmented regions. Because we were primarily interested in measuring interaction between the spindle and the cell cortex, it was necessary to develop a reliable method of denoting spindle poles. We can use the stereotyped morphology of *Xenopus* mitotic spindles to our advantage, in that the spindle poles are located at the ends of the long axis of the spindle. Thus spindle pole location can be estimated as the extrema of the fitted ellipse along the major axis (Supplemental Figure S4C). As an alternative approach, pole location can be measured as the point on the region perimeter farthest from the region centroid in the direction of the major axis. This method, although more prone to error from noise due to slight variation in frame-to-frame segmentation, is more accurate in the rare circumstance in which the spindle appears nonelliptical or bent.

Once the location of the spindle poles was determined, distance to the cell boundary was measured in three different ways. The first was to find the point on the cell outline that is nearest the spindle pole (Supplemental Figure S4D). This was accomplished by calculating the distance from the spindle pole to every valid point on the cell boundary, excluding those that would cross the spindle midline, and choosing the closest. The second was to find locations on the cell boundary that lay along the long axis of the spindle. This was accomplished by converting the locations of the spindle poles and cell boundary pixels from a Cartesian to polar coordinate system around the spindle centroid and choosing the boundary points that lay along the spindle axis. The third was to calculate the distance between the spindle pole and the cortical point along the anaphase axis of the cell.

Automated recognition of temporal landmarks

To relate the spatial dynamics of the spindle to mitotic progression, quantitative criteria for the definition of NEB, metaphase, and anaphase onset were implemented by using the same general principles used to define NEB, metaphase, and anaphase described earlier. Specifically, to calculate the frame of nuclear envelope breakdown within a time series, the average tubulin signal within the DNA region for all available frames was corrected for same-cell tubulin background and normalized to a maximum of 1 (Supplemental Figure S5A). As expected, the tubulin signal in the DNA region is typically at or below background preceding NEB. After NEB, the tubulin signal increases quickly to its maximum levels. However, bright foci of tubulin are often associated with the nuclear region in the time immediately preceding NEB. To account for this, we set a threshold of one-third maximum tubulin signal as the criterion for denoting time of NEB.

To identify metaphase, we used two complementary metrics of the ellipse fit to the DNA region: eccentricity and minor axis length. Eccentricity is the ratio of interfoci length to major axis length. A circle has an eccentricity of 0, and a line has an eccentricity of 1. Thus a pre-NEB nucleus, which is generally round, will have a low eccentricity, whereas a metaphase plate will have an eccentricity approaching 1. We find that an eccentricity threshold of within 5% of maximum corresponds well to what appears to be a metaphase plate by eye (Supplemental Figure S5B). However, eccentricity is a measure of relative, not absolute, size. It is therefore necessary to include an absolute size threshold. To do this, we measure the minor axis length of the fit ellipse, which corresponds to the width of the metaphase plate. We consider a metaphase plate to be within about 1 µm of the narrowest minor axis length. Note that this measure of metaphase does not account for blatantly misaligned chromosomes, as it is defined using the region to which the morphological reconstruction filter has been applied. Misaligned chromosomes, uncovered by comparing the ratio of area in the morphologically reconstructed and nonreconstructed histone objects, are accounted for separately from development of the metaphase plate. This is done because, as seen in Supplemental Figure S3A, misaligned chromosomes can be present in the context of an otherwise normal-appearing metaphase mitotic spindle. We expect the intracellular forces acting on the spindle, and resultant spindle dynamics, to be more similar to a metaphase spindle than a premetaphase spindle.

Finally, we set quantitative criteria for anaphase onset based on eccentricity of the elliptical fit to the histone region. As the chromosomes begin to separate at anaphase onset, the eccentricity decreases (Supplemental Figure S5B). Then eccentricity increases again as the chromosomes pull toward the edge of the cell, resulting in an elliptical region roughly perpendicular to the former metaphase plate. Anaphase onset can thus be identified as a 5% decrease from maximum during the transient drop in eccentricity (Supplemental Methods).

All thresholds were chosen initially to approximately mimic manual annotations. To further optimize these thresholds, they were systematically varied, and the time differences between automatically annotated times of NEB, metaphase, and anaphase were compared with manual annotations. Time difference and standard error of time difference between manually and automatically selected frames were examined for 106 mitotic cells (Supplemental Figure S5, C–E). A threshold that perfectly mimics manual annotation would result in time differences and SDs of 0. However, because manual annotation is error prone, some measure of judgment is still necessary in balancing the minimization of standard error, maximization of percentage detection, and recapitulation, or improvement on, manual annotation. By these three metrics and visual inspection of H2B eccentricity and tubulin density plots for all 106 spindles, we determined that the initially chosen thresholds are appropriate.

NEB, metaphase, and anaphase were successfully determined in 100 of 106 mitotic cells. From these, the time intervals of NEB–anaphase, NEB–metaphase, and metaphase–anaphase were then compared between manual and automated annotation methods (Supplemental Figure S5F). Although significant differences can be detected in NEB–anaphase interval and metaphase–anaphase interval (both $p < 0.001$, paired t test), we consider these differences to be of little biological relevance, considering the large size of the data set. Difference in NEB–metaphase interval was not significantly different ($p = 0.2$, paired t test). From visual inspection of the results, additional outliers were generated in the automated intervals that include metaphase, indicating a higher level of error in this measurement and confirming our prior observation that metaphase is the most difficult mitotic stage to recognize in an automated manner.

Code availability

The Spindlometer MatLab program will be made available by email upon request.

ACKNOWLEDGMENTS

We thank Rodrigo Fernandez-Gonzalez for providing the code for the LiveWire and MEDUSA programs. This work was supported by National Institutes of Health Grant GM52932 to W.M.B., National Research Service Award F30CA189673 to M.E.L., and National Institutes of Health Instrumentation Grant 1S10RR026729-01 (K. Eliceiri, principal investigator). M.E.L. was supported by Grant T32GM008692 for the University of Wisconsin Medical Scientist Training Program.

REFERENCES

Adames NR, Cooper JA (2000). Microtubule interactions with the cell cortex causing nuclear movements in Saccharomyces cerevisiae. J Cell Biol 149, 863–874.

Adams RJ (1996). Metaphase spindles rotate in the neuroepithelium of rat cerebral cortex. J Neurosci 16, 7610–7618.

Baena-López LA, Baonza A, García-Bellido A (2005). The orientation of cell divisions determines the shape of Drosophila organs. Curr Biol 15, 1640–1644.

Berg J, Derfler B, Pennisi C, Corey D, Cheney RE (2000). Myosin-X, a novel myosin with pleckstrin homology domains, associates with regions of dynamic actin. J Cell Sci 113, 3439–3451.

Bergstralh DT, Lovegrove HE, Kujawiak I, Dawney NS, Zhu J, Cooper S, Zhang R, St Johnston D (2016). Pins is not required for spindle orientation in the Drosophila wing disc. Development 143, 2573–2581.

Bergstralh DT, Lovegrove HE, St Johnston D (2013). Discs large links spindle orientation to apical-basal polarity in Drosophila epithelia. Curr Biol 23, 1707–1712.

Betschinger J, Knoblich JA (2004). Dare to be different: asymmetric cell division in Drosophila, C. elegans and vertebrates. Curr Biol 14, R674–R685.

Bosveld F, Markova O, Guirao B, Martin C, Wang Z, Pierre A, Balakireva M, Gaugue I, Ainslie A, Christophorou N, *et al.* (2016). Epithelial tricellular junctions act as interphase cell shape sensors to orient mitosis. Nature 530, 495–498.

Campinho P, Behrndt M, Ranft J, Risler T, Minc N, Heisenberg C-P (2013). Tension-oriented cell divisions limit anisotropic tissue tension in epithelial spreading during zebrafish epiboly. Nat Cell Biol 15, 1405–1414.

Castanon I, Abrami L, Holtzer L, Heisenberg CP, van der Goot FG, González-Gaitán M (2013). Anthrax toxin receptor 2a controls mitotic spindle positioning. Nat Cell Biol 15, 28–39.

Caydasi AK, Kurtulmus B, Orrico MIL, Hofmann A, Ibrahim B, Pereira G (2010). Elm1 kinase activates the spindle position checkpoint kinase Kin4. J Cell Biol 190, 975–989.

Clarke S, Vogel JP, Deschenes RJ, Stock J (1988). Posttranslational modification of the Ha-ras oncogene protein: evidence for a third class of protein carboxyl methyltransferases. Proc Natl Acad Sci USA 85, 4643–4647.

Cluet D, Stébé P-N, Riche S, Spichty M, Delattre M (2014). Automated high-throughput quantification of mitotic spindle positioning from DIC movies of Caenorhabditis embryos. PLoS One 9, e93718.

Collins ES, Balchand SK, Faraci JL, Wadsworth P, Lee W-L (2012). Cell cycle-regulated cortical dynein/dynactin promotes symmetric cell division by differential pole motion in anaphase. Mol Biol Cell 23, 3380–3390.

Corrigan AM, Shrestha RL, Zulkipli I, Hiroi N, Liu Y, Tamura N, Yang B, Patel J, Funahashi A, Donald A, *et al.* (2013). Automated tracking of mitotic spindle pole positions shows that LGN is required for spindle rotation but not orientation maintenance. Cell Cycle 12, 2643–2655.

da Silva SM, Vincent J-P (2007). Oriented cell divisions in the extending germband of Drosophila. Development 134, 3049–3054.

Decarreau J, Driver J, Asbury C, Wordeman L (2014). Rapid measurement of mitotic spindle orientation in cultured mammalian cells. Methods Mol Biol 1136, 31–40.

Fernandez-Gonzalez R, Zallen JA (2011). Oscillatory behaviors and hierarchical assembly of contractile structures in intercalating cells. Phys Biol 8, 045005.

Fischer E, Legue E, Doyen A, Nato F, Nicolas J-F, Torres V, Yaniv M, Pontoglio M (2006). Defective planar cell polarity in polycystic kidney disease. Nat Genet 38, 21–23.

Fleming ES, Temchin M, Wu Q, Maggio-Price L, Tirnauer JS (2009). Spindle misorientation in tumors from APC(min/+) mice. Mol Carcinog 48, 592–598.

Fleming ES, Zajac M, Moschenross DM, Montrose DC, Rosenberg DW, Cowan AE, Tirnauer JS (2007). Planar spindle orientation and asymmetric cytokinesis in the mouse small intestine. J Histochem Cytochem 55, 1173–1180.

Gibson WT, Veldhuis JH, Rubinstein B, Cartwright HN, Perrimon N, Brodland GW, Nagpal R, Gibson MC (2011). Control of the mitotic cleavage plane by local epithelial topology. Cell 144, 427–438.

Gong Y, Mo C, Fraser SE (2004). Planar cell polarity signalling controls cell division orientation during zebrafish gastrulation. Nature 430, 689–693.

Grenfell AW, Strzelecka M, Crowder ME, Helmke KJ, Schlaitz A-L, Heald R (2016). A versatile multivariate image analysis pipeline reveals features of Xenopus extract spindles. J Cell Biol 213, 127–136.

Hancock JF, Magee AI, Childs JE, Marshall CJ (1989). All ras proteins are polyisoprenylated but only some are palmitoylated. Cell 57, 1167–1177.

Haydar TF, Ang E, Rakic P (2003). Mitotic spindle rotation and mode of cell division in the developing telencephalon. Proc Natl Acad Sci USA 100, 2890–2895.

Hertwig O (1884). Das problem der befruchtung und der isotropie des eies, eine theorie der vererbung. Jen Z Naturwiss 18. 276–318.

Hirano Y, Hatano T, Takahashi A, Toriyama M, Inagaki N, Hakoshima T (2011). Structural basis of cargo recognition by the myosin-X MyTH4-FERM domain. EMBO J 30, 2734–2747.

Ikenouchi J, Furuse M, Furuse K, Sasaki H, Tsukita S, Tsukita S (2005). Tricellulin constitutes a novel barrier at tricellular contacts of epithelial cells. J Cell Biol 171, 939–945.

Jüschke C, Xie Y, Postiglione MP, Knoblich JA (2014). Analysis and modeling of mitotic spindle orientations in three dimensions. Proc Natl Acad Sci USA 111, 1014–1019.

Kiyomitsu T, Cheeseman IM (2012). Chromosome- and spindle-pole-derived signals generate an intrinsic code for spindle position and orientation. Nat Cell Biol 14, 311–317.

Kiyomitsu T, Cheeseman IM (2013). Cortical dynein and asymmetric membrane elongation coordinately position the spindle in anaphase. Cell 154, 391–402.

Knoblich JA (2001). Asymmetric cell division during animal development. Nat Rev Mol Cell Biol 2, 11–20.

Knoblich JA (2008). Mechanisms of asymmetric stem cell division. Cell 132, 583–597.

Kotak S, Busso C, Gönczy P (2012). Cortical dynein is critical for proper spindle positioning in human cells. J Cell Biol 199, 97–110.

Kwon M, Bagonis M, Danuser G, Pellman D (2015). Direct microtubule-binding by Myosin-10 orients centrosomes toward retraction fibers and subcortical actin clouds. Dev Cell 34, 323–337.

Laan L, Pavin N, Husson J, Romet-Lemonne G, van Duijn M, López MP, Vale RD, Jülicher F, Reck-Peterson SL, Dogterom M (2012). Cortical dynein controls microtubule dynamics to generate pulling forces that position microtubule asters. Cell 148, 502–514.

Linkert M, Rueden CT, Allan C, Burel J-M, Moore W, Patterson A, Loranger B, Moore J, Neves C, Macdonald D, *et al.* (2010). Metadata matters: access to image data in the real world. J Cell Biol 189, 777–782.

Moore JK, Chudalayandi P, Heil-Chapdelaine RA, Cooper JA (2010). The spindle position checkpoint is coordinated by the Elm1 kinase. J Cell Biol 191, 493–503.

Morin X, Bellaïche Y (2011). Mitotic spindle orientation in asymmetric and symmetric cell divisions during animal development. Dev Cell 21, 102–119.

Morin X, Jaouen F, Durbec P (2007). Control of planar divisions by the G-protein regulator LGN maintains progenitors in the chick neuroepithelium. Nat Neurosci 10, 1440–1448.

Nédélec F, Surrey T, Maggs AC (2001). Dynamic concentration of motors in microtubule arrays. Phys Rev Lett 86, 3192–3195.

Nestor-Bergmann A, Goddard G, Woolner S (2014). Force and the spindle: mechanical cues in mitotic spindle orientation. Semin Cell Dev Biol 34, 133–139.

O'Connell CB, Wang YL (2000). Mammalian spindle orientation and position respond to changes in cell shape in a dynein-dependent fashion. Mol Biol Cell 11, 1765–1774.

Oda Y, Otani T, Ikenouchi J, Furuse M (2014). Tricellulin regulates junctional tension of epithelial cells at tricellular contacts through Cdc42. J Cell Sci 127, 4201–4212.

Otsu N (1979). A threshold selection method from gray-level histograms. IEEE Trans Syst Man Cybern 9, 62–66.

Peyre E, Jaouen F, Saadaoui M, Haren L, Merdes A, Durbec P, Morin X (2011). A lateral belt of cortical LGN and NuMA guides mitotic spindle movements and planar division in neuroepithelial cells. J Cell Biol 193, 141–154.

Reyes CC, Jin M, Breznau EB, Espino R, Delgado-Gonzalo R, Goryachev AB, Miller AL (2014). Anillin regulates cell-cell junction integrity by organizing junctional accumulation of Rho-GTP and actomyosin. Curr Biol 24, 1263–1270.

Roszko I, Afonso C, Henrique D, Mathis L (2006). Key role played by RhoA in the balance between planar and apico-basal cell divisions in the chick neuroepithelium. Dev Biol 298, 212–224.

Schindelin J, Arganda-Carreras I, Frise E, Kaynig V, Longair M, Pietzsch T, Preibisch S, Rueden C, Saalfeld S, Schmid B, *et al*. (2012). Fiji: an open-source platform for biological-image analysis. Nat Methods 9, 676–682.

Siller KH, Cabernard C, Doe CQ (2006). The NuMA-related Mud protein binds Pins and regulates spindle orientation in Drosophila neuroblasts. Nat Cell Biol 8, 594–600.

Strauss B, Adams RJ, Papalopulu N (2006). A default mechanism of spindle orientation based on cell shape is sufficient to generate cell fate diversity in polarised Xenopus blastomeres. Development 133, 3883–3893.

Subach OM, Gundorov IS, Yoshimura M, Subach FV, Zhang J, Grüenwald D, Souslova E, Chudakov DM, Verkhusha VV (2008). Conversion of red fluorescent protein into a bright blue probe. Chem Biol 15, 1116–1124.

Tarantino N, Tinevez J-Y, Crowell EF, Boisson B, Henriques R, Mhlanga M, Agou F, Israël A, Laplantine E (2014). TNF and IL-1 exhibit distinct ubiquitin requirements for inducing NEMO-IKK supramolecular structures. J Cell Biol 204, 231–245.

Théry M, Jiménez-Dalmaroni A, Racine V, Bornens M, Jülicher F (2007). Experimental and theoretical study of mitotic spindle orientation. Nature 447, 493–496.

Théry M, Racine V, Pépin A, Piel M, Chen Y, Sibarita J-B, Bornens M (2005). The extracellular matrix guides the orientation of the cell division axis. Nat Cell Biol 7, 947–953.

Toyoshima F, Nishida E (2007). Integrin-mediated adhesion orients the spindle parallel to the substratum in an EB1- and myosin X-dependent manner. EMBO J 26, 1487–1498.

Wang C, Li S, Januschke J, Rossi F, Izumi Y, Garcia-Alvarez G, Gwee SS, Soon SB, Sidhu HK, Yu F, *et al*. (2011). An ana2/ctp/mud complex regulates spindle orientation in Drosophila neuroblasts. Dev Cell 21, 520–533.

Weber KL, Sokac AM, Berg JS, Cheney RE, Bement WM (2004). A microtubule-binding myosin required for nuclear anchoring and spindle assembly. Nature 431, 325–329.

Willumsen B, Christensen A (1984). The p21 ras C-terminus is required for transformation and membrane association. Nature 310, 583–586.

Woolner S, O'Brien LL, Wiese C, Bement WM (2008). Myosin-10 and actin filaments are essential for mitotic spindle function. J Cell Biol 182, 77–88.

Woolner S, Papalopulu N (2012). Spindle position in symmetric cell divisions during epiboly is controlled by opposing and dynamic apicobasal forces. Dev Cell 22, 775–787.

Zulueta-Coarasa T, Tamada M, Lee EJ, Fernandez-Gonzalez R (2014). Automated multidimensional image analysis reveals a role for Abl in embryonic wound repair. Development 141, 2901–2911.